Modelling Negative Linear Compressibility in Tetragonal Beam Structures

Barnes D.L., Miller W., Evans K.E. and Marmier A.*

College of Engineering Mathematics and Physical Science, University of Exeter, UK, EX4 4QF, England

Abstract

Most materials compress axially in all directions when loaded hydrostatically. Contrary to this, some materials have been discovered that exhibit negative linear compressibility and, as such, expand along a specific axis or plane. This paper analyses a fundamental mechanism by using a combination of finite element simulations and analytical derivations to show that negative linear compressibility can be found in a body-centred or face-centred tetragonal network of nodes connected by a network of beams. The magnitude and direction of this behaviour depends on the cross geometry in the network.

Keywords:

Negative linear compressibility

Beam structure

Anisotropic elasticity

Finite element

Tetragonal

Stretch densification

*: Corresponding Author: a.s.h.marmier@ex.ac.uk

1 Introduction

Abnormal elastic properties have received a large amount of interest in the last two decades, driven in part by potential applications, and by the availability of new manufacturing methods. The theory of elasticity still contains some surprises, as evidenced by the realisation that the majority of cubic metals are auxetic (exhibit a Negative Poisson's Ratio, NPR) in the [110] direction(Baughman et al., 1998a), a property previously thought to be confined to few systems(Yang et al., 2004). Recent developments(Ting and Chen, 2005) have revealed the complexity of the cubic symmetry, where a change in the direction of the extreme values of Poisson's ratio from the [110] direction to near the [111] direction occurs for some combinations of the three elastic constants. Beside NPR, some materials can display negative linear compressibility (NLC) and in some cases negative area compressibility (NAC), and bizarrely do not contract in all directions but expand in one or two directions when subjected to hydrostatic pressure(Baughman et al., 1998b). This property appears to be rare in natural materials, on the other hand, it is evident that a wine rack type structure would show NLC as illustrated in Fig. 1. Interestingly, the equation describing linear compressibility is the transpose of that describing volume change under pure normal stress: materials with NLC can also be called stretch densified. In other words, NLC require Poisson's ratio to be large, larger than 0.5 on the axis of NLC.

It is still an early stage for applications, but it is possible to envisage composites with zero compressibility, or pressure driven actuators as in nanotubes based artificial muscles(Aliev et al., 2009) or sensors, as well as acoustic damping.

Compressibilities are defined by relative change in length, area or volume when subjected to hydrostatic pressure. The linear compressibility β_L, area compressibility β_A and volume compressibility β_V are $-dL/LdP$, $-dA/AdP$, and $-dV/VdP$ where P is the applied hydrostatic pressure, L is the length, A is area and V is the volume . Negative values of volume compressibility are thermodynamically impossible(Nye, 1985), but tenuous evidence to the contrary exists where a strain dependant NVC (negative volume compressibility) has been encountered in foams(Lakes and Drugan, 2002) and in networks of bi-materials where the hydrostatic pressure was subjected to all interior and exterior faces(Gatt and Grima, 2008). However negative values of the other two properties have unquestionably been identified in crystals.

Baughman originally theorised the property could be present in hypothetical carbon phases via molecular mechanics simulations(Baughman and Galvao, 1993) and later identified the presence of NLC in 13 different crystals of various symmetries from analysis of published elastic

constants(Baughman et al., 1998b). Of the approximately five hundred of materials checked, two, mercurous iodide and mercurous bromide, were of tetragonal symmetry, making tetragonal the simplest crystal symmetry able to support NLC. Recent *ab initio* calculations(Marmier et al., 2010) have shown that platinum sulphide in its tetragonal phase (cooperite) has NLC. Neutron diffraction tests(Goodwin et al., 2008) have been conducted to determine the hydrostatic deformation of silver hexaconocobaltate. It was observed to have large NLC in a trigonal phase and a post phase-transition monoclinic phase. The same technique has also proved the presense of NLC in methanol monohydrate(Fortes et al., 2011). Other materials have been shown to have NLC triggered by a pressure induced phase transition, molecular dynamic simulations show that hydrocarbon chains will experience a very pronounced phase change under high hydrostatic loading that leads to the chains suddenly becoming aligned thus causing an expansion on a particular axis(Skvortsov et al., 2007). Paratellurite was shown to exhibit NLC(Skelton et al., 1976) due to a phase transition induced by increased pressure where the symmetry changes from a tetragonal to an orthorhombic structure at 8kbar. During this orthorhombic phase, a small NLC was present between 8 and 90kbars. The possibility of Carbon nanotube sheets exhibiting NLC has also been investigated using analytical derivations(Coluci et al., 2008; Hall et al., 2008). Several naturally occurring NLC structures have also been discovered. The muscular hydrostats of squid tentacles, worms and some snakes exhibit NLC(Oreilly et al., 1997). Additionally, the thickness of lipid bilayers increases when subjected to hydrostatic loading(Braganza and Worcester, 1986; White and King, 1985).

Structurally, one of the mechanisms causing this abnormal effect, the "wine rack mechanism" proposed by Baughman et al. and depicted in Fig. 1 shows that a simple array of beams stretch densifies under axial loading. FE simulations(Weng et al., 2008) have been performed on both 2D and 3D crosses using a composite material with rectangular and tetragonal unit cells. Solid crosses running across the body of the unit cell with a filler material are assigned varying material properties for varying unit cell aspect ratios. Maximum normalised (ratio of linear to area compressibility) NLC was observed in the 2D models for unit cells of aspect ratios approaching one, while 3D results yield maximum NLC values at aspect ratios close to two, but no mechanism for this behaviour was proposed. Analytical calculations(Grima et al., 2008) have also proven that NLC and NAC can be generated in truss networks composed of beams sets of differing stiffness. Additionally, FE simulations of bi-material beams(Gatt et al., 2009) where materials of different Young's moduli and Poisson's ratio are bonded together can exhibit NLC. Recently NLC has been proved to be a property of hexagonal honeycombs with aspect ratio not equal to one(Grima et al., 2011).

NLC is present in several classes of crystal systems, but notably not in cubic crystals. This is not surprising as, for cubic symmetries linear compressibility is isotropic (and therefore positive as volume compressibility must be positive)(Nye, 1985). The elastically simplest systems that can have NLC are tetragonal and hexagonal.

The structure of the paper is as follows. Section 2 introduces the structure and beam nomenclature of the frameworks and details the computational and analytical methodologies. The results for the 2D rectangular models are presented and discussed in Section 3.2, and those for the 3D tetragonal models in Section 3.2. Finally we conclude in Section 4.

2 Methodology

2.1 Framework Structures

2.1.1 2D Rectangular

Figure 2(a)-2(c) shows the 2D rectangular model comprising nodes positioned at the corners of the unit cell and illustrates the arrangement of first nearest neighbour (type Ia and type Ib) and second nearest neighbour (type II) beams. Structures consisiting of type I and type II beams are analysed separately, the models are studied for varying angles of θ which also modify the aspect ratio of the unit cell. The length of the beams being tested is kept constant for different ratios to ensure that the ratio between its flexure and compressive resistances remains unchanged. The model is made of 1D beams which are assigned arbitrary lengths of 0.1m and radii of 0.005m with a Young's modulus of 10MPa.

2.1.2 3D Tetragonal

Fig. 2(d)-(g) show the layout of the 3D tetragonal model, which is a combination of simple tetragonal (type Ia and type Ib), face centred tetragonal (type IIa and IIb) and body centred tetragonal (type III) beams based around tetragonal unit cells of varying aspect ratios. Similarly to the 2D model, the angle θ is modified and γ, which is used in the analytical formula, varies as a consequence of changing θ. The beam length remains constant for different values of θ in order to keep the ratio between the flexure and compressive resistances constant.

2.2 Identifying NLC / NAC

2.2.1 2D Rectangular Model

The linear compressibility of the 2D model is determined from elastic compliances using the equation,

$$\beta_L = S_{11} + S_{12} - (S_{11} - S_{22})L_y^2 , \quad (1)$$

where the S_{ij} are the components of the compliance matrix in Voigt notation and L_y is the y component of the unit vector (dimensionless) in the direction the compressibility is being measured. Extreme values lie on the principal axes and the formula can be simplified to find these limiting values for the absolute linear compressibility in the x direction, $\beta_{Lx} = S_{11} + S_{12}$, and in the y direction, $\beta_{Ly} = S_{22} + S_{12}$. Additionally, the area compressibility β_A is the sum of these two compressibilities. Note that in the 2D case, the compressibilities and compliances are expressed in $m.N^{-1}$, i.e. the inverse of a 2D stress or pressure –a force over a length–.

2.2.2 3D Tetragonal Model

Linear compressibilities for tetragonal frameworks can also be determined from elastic constants. The formula for the linear compressibility within a tetragonal system(Nye, 1985) is,

$$\beta_L = S_{11} + S_{12} + S_{13} - (S_{11} + S_{12} - S_{13} - S_{33})L_z^2 . \quad (2)$$

The two extrema are attained for values of the z component of the unit vector L_z equal to one and zero. Eqs. (3) and (4) show formulae for these extremes. Additionally, any negative values observed on the x or y axis will be common to both directions, therefore creating NAC on the xy plane. The orthogonal linear compressibilities are defined as,

$$\beta_{Ly} = \beta_{Lx} = S_{11} + S_{12} + S_{13} , \quad (3)$$

and

$$\beta_{Lz} = 2S_{13} + S_{33} . \quad (4)$$

Eqs. (3) and (4) are used to calculate the *absolute* value of the linear compressibility. While this is a useful quantity, it might hide the fact that the negative effect is small compared to the overall dimension changes. Therefore it is also a good idea to calculate the normalised linear compressibility which is defined by $\beta_{LN} = \beta_L / \beta_A$ for the 2D case and by $\beta_{LN} = \beta_L / \beta_V$ for the 3D case, where the volume compressibility is the sum of the three orthogonal linear compressibilities, $\beta_V = \beta_{Lx} + \beta_{Ly} + \beta_{Lz}$.

2.3 Extracting Compliances from FE models

FE simulations of different boundary condition sets are applied to find the required compliances. A 5×5×5 array of unit cells is used for each analysis set where forced deflections of 0.001% strain are

applied and reaction forces at the loaded faces are summed to determine the compliances. Eqs (1) and (2) are used to calculate absolute linear compressibilities from these compliances.

Abaqus 6.9(2010) is used to perform the finite element analysis and beams are modelled by B31 type linear beam elements. Linear elastic material properties are assigned to the model as appropriate for small strain linear elastic simulations.

2.4 Analytical Methodology

An analytical model has been developed for comparison with the finite element simulations. It uses classical beam theory(Gere and Timoshenko, 1996) and models the behaviour of the various arrangements. The model was built up with a hydrostatic load acting on the faces of a single unit cell where the associated forces only acted on nodes occupying the borders of the unit cell. The couple of forces on each beam can then be resolved into axial or radial components. The axial components lead to a compression of the beams, following a straightforward application of Hooke's law. The radial components create bending in the beams, resisted by their second moment of area. Fig. 2 details the parameters of the models.

3 Results and Discussion

3.1 2D Results

The following analytical expressions can been derived for the absolute linear compressibility of the type II beams of the 2D model,

$$\beta_y = -\left[\frac{L^3\cot(\theta)\left(\cos^2(\theta)-\sin^2(\theta)\right)}{3EI}+\frac{2L\sin(\theta)\cos(\theta)}{EA}+\frac{L^3\left(\cos^2(\theta)-\sin^2(\theta)\right)}{3EI}\tan\left(\frac{PL^3\left(\cos^2(\theta)-\sin^2(\theta)\right)}{2EI}\right)\right] \quad (5)$$

and

$$\beta_x = \left[\frac{L^3\tan(\theta)\left(\cos^2(\theta)-\sin^2(\theta)\right)}{3EI}-\frac{2L\sin(\theta)\cos(\theta)}{EA}+\frac{L^3\left(\cos^2(\theta)-\sin^2(\theta)\right)}{3EI}\tan\left(\frac{PL^3\left(\cos^2(\theta)-\sin^2(\theta)\right)}{2EI}\right)\right] \quad (6)$$

where E is the Young's modulus, L is length of the beam, A is the area of the constituent beams, I is the second moment of area and P is the applied 2D hydrostatic pressure (units $N.m^{-1}$). The thirds term represents the axial deflection due to bending and can be neglected at small pressure for small deflection and the linear compressiblities can be simplified to

$$\beta_y = \frac{L^3\cot(\theta)\left(\cos^2(\theta)-\sin^2(\theta)\right)}{3EI}+\frac{2L\sin(\theta)\cos(\theta)}{EA} \quad (7)$$

and

$$\beta_x = -\frac{L^3 \tan(\theta)\left(\cos^2(\theta)-\sin^2(\theta)\right)}{3EI} + \frac{2L\sin(\theta)\cos(\theta)}{EA}. \quad (8)$$

Fig. 3 displays the results from both the FE and analytical methodologies, but only one graph is illustrated as agreement between these two models is excellent, within 1.5×10^{-4}%. Results are symmetric around 45° with the direction of minimum linear compressibility changing from the *x* direction to the *y* direction at 45° and maximum absolute values of NLC occurring at θ=25.9°and θ=64.1°. These angles correspond to an aspect ratio of 2.06, very close to, but not quite, two. Normalised values of linear compressibility show a minimum at aspect ratios not quite equal to one ($\theta\approx$45°.), which can be attributed to the decreasing area compressibility –almost to zero– of the structure as the aspect ratio approaches one. This effect is due to the alignment of the beams into the direction of the hydrostatic load, making the deformation of type II beams dominated by axial compression instead of bending, and therefore very small. Let us note that outside this high-symmetry zone, positive linear compressibilities are larger than the negative values for all structures as shown by the low values of normalised NLC: for instance, at θ=25.9°, the minimum relative compressibility is around -0.33, which means that the magnitude of the maximum absolute compressibility is four time larger than that of the minimum absolute compressibility.

The inclusion of type I beams only diminishes the negative effect. The mechanism is conceptually very close to the wine-rack model, with beam bending at nodes replacing hinging. In both cases, it is the symmetry breaking (cubic to rectangular) which allows beam bending (or hinging) and subsequent NLC.

3.2 3D Tetragonal Results

3.2.1 Type III Beam structure

Analytical expressions for linear compressibilities have also been derived for a structure composed exclusively of type III beams an the relationships are as follows,

$$\beta_y = \beta_y = \frac{\left(2L^4\sin^3(\gamma)\right)-\left(L^4\sin(\gamma)\cos^2(\gamma)\right)}{6EI} - \frac{\left(3L^2\sin(\gamma)\cos^2(\gamma)\right)}{2EA} \quad (9)$$

and

$$\beta_z = \frac{\left(2L^4\sin^2(\gamma)\cos^2(\gamma)\right)-\left(L^4\cos^4(\gamma)\right)}{6EI\sin(\gamma)} - \frac{\left(3L^2\sin(\gamma)\cos^2(\gamma)\right)}{2EA} \quad (10)$$

Normalised values can also be derived by dividing the linear compressibility by the volume

compressibility, calculated by summing the three linear compressibilities,

$$\beta_V = 2\beta_x + \beta_z \,,\ \beta_{xN} = \frac{\beta_x}{\beta_V} \,,\ \beta_{zN} = \frac{\beta_z}{\beta_V} \,. \tag{11}$$

As in the 2D case, the analytical and FE models show almost perfect agreement and the results are displayed in Fig. 4 for both normalised and absolute values of linear compressibility. While γ is the natural variable for this structure, for consistency and ease of comparison, Fig.4 expresses the compressibilities as functions of the angle θ. These 3D results are not symmetric around 45° as with the 2D case because of the transition from a negative area compressibility to a negative linear compressibility at 45° and from acting in the *xy* lane to acting in the *z* direction. This makes the effect more pronounced but in a much smaller range of directions. Similarly to the 2D results, the maximum negative absolute values occur at θ=26.6° and θ=61.2° (aspect ratio close to two) while normalised values are at a maximum at aspect ratios close too, but not equal to one.

3.2.2 Type IIa Beam structure

A structures composed of type II beams are only capable of supporting NLC when the type IIb beams (top and bottom of tetragon) are not present because a hydrostatic pressure only loads these beams in compression, due their square symmetry. As a consequence, the type IIa beams are constrained and not allowed to bend. Fig. 5 shows the normalised and absolute linear compressiblities of the type IIa structure for different angles of θ and the analytical formulae are given as follows,

$$\beta_x = \beta_y = \left(\frac{L^4 \sin(\theta)\cos^2(\theta)}{6EI} - \frac{L^4 \sin^2(\theta)}{3EI} \right) - \frac{3L^2 \sin(\theta)\cos^2(\theta)}{2EA} \tag{12}$$

And

$$\beta_z = -\left(\frac{L^4 \cot(\theta)\cos^3(\theta)}{6EI} - \frac{L^4 \sin(\theta)\cos^2(\theta)}{3EI} \right) - \frac{3L^2 \sin(\theta)\cos^2(\theta)}{2EA} \tag{13}$$

The behaviour of this structure differs slightly to that of the type III arrangement. As S_{33} is larger due to the removal of the type IIb beams, the angle at which the structure is isotropic is much shallower and occurs at θ=35°, which also means that absolute peak NLC occurs at shallower angles θ=19.4° and θ=52.1° instead of 26.6° and 61.2°. At first sight, it might seem surprising that a clearly tetragonal cell (35° corresponds to an aspect ratio of 0.7) is elastically isotropic, but the symmetry of the elastic tensor is not necessarily the same as that of the periodic unit cell.

3.2.3 Modifying Beam Aspect ratio

NLC is dependent on the tendency of the beams forming the structure to bend as opposed to deform axially. Therefore, by decreasing the constituent beams' second moment of area with respect to their cross sectional area (by modifying their length/radius aspect ratio) the NLC effect can be increased. The 3D analytical model was used to determine how NLC could be made larger by increasing the length/radius aspect ratio for two different values of the angle θ.

Fig. 6 shows that the absolute values of minimum linear compressibility decrease indefinitely as constituent beam aspect ratio are increased, while there is no appreciable change in normalised values across this change in beam aspect ratio. Additionally, increasing the Young's modulus of the constituent beams decreases the absolute NLC of the structures but does not affect the normalised values.

It should therefore be possible to fit the linear compressibilities of real crystals to combinations of beams of specific aspect ratios and Young's moduli, but we do not think such an exercise would be very informative when the bond structure of the tetragonal crystals exhibiting NLC differs from the simple arrangements described here.

4 Conclusion

In this work, we have used finite element analysis to show that a tetragonal structure composed of a network of bending beams can exhibit negative linear compressibility in one or two directions. We have identified the mechanism responsible and developed an analytical model based on beam theory in two and three dimensions that replicates and explains finite elements results. The main drivers for NLC are intersecting beams, and it is the intersecting angle that controls how negative linear compressibility can be. The optimum angle for maximum absolute NLC is 25.9º or 64.1º for 2D structures while for 3D type III this is slightly changed to 26.6° and 61.2°. Additionally maximum relative NLC (scaled by the volumetric compressibility) is obtained for angles close (but not equal) to 45° for both 3D type III and 2D type II but for angles of θ close to 35° for the 3D type II beams. The aspect ratio of the constituent beams affects magnitude of absolute NLC. This suggests ways to tailor framework structures optimised for NLC.

References

2010. Abaqus 6.9-3, Simulia, 6.9-3 ed. Dassault.
Aliev, A.E., Oh, J.Y., Kozlov, M.E., Kuznetsov, A.A., Fang, S.L., Fonseca, A.F., Ovalle, R., Lima, M.D., Haque, M.H., Gartstein, Y.N., Zhang, M., Zakhidov, A.A., Baughman, R.H., 2009. Giant-Stroke, Superelastic Carbon Nanotube Aerogel Muscles. Science 323, 1575-1578.
Baughman, R.H., Galvao, D.S., 1993. Crystalline Networks with Unusual Predicted Mechanical and Thermal-Properties. Nature 365, 735-737.
Baughman, R.H., Shacklette, J.M., Zakhidov, A.A., Stafstrom, S., 1998a. Negative Poisson's ratios as a common feature of cubic metals. Nature 392, 362-365.
Baughman, R.H., Stafstrom, S., Cui, C.X., Dantas, S.O., 1998b. Materials with negative compressibilities in one or more dimensions. Science 279, 1522-1524.
Braganza, L.F., Worcester, D.L., 1986. Structural-Changes in Lipid Bilayers and Biological-Membranes Caused by Hydrostatic-Pressure. Biochemistry 25, 7484-7488.
Coluci, V.R., Hall, L.J., Kozlov, M.E., Zhang, M., Dantas, S.O., Galvao, D.S., Baughman, R.H., 2008. Modeling the auxetic transition for carbon nanotube sheets. Physical Review B 78.
Fortes, A.D., Suard, E., Knight, K.S., 2011. Negative Linear Compressibility and Massive Anisotropic Thermal Expansion in Methanol Monohydrate Science 331, 742-746
Gatt, R., Attard, D., Grima, J.N., 2009. On the behaviour of bi-material strips when subjected to changes in external hydrostatic pressure. Scripta Materialia 60, 65-67.
Gatt, R., Grima, J.N., 2008. Negative compressibility. Physica Status Solidi-Rapid Research Letters 2, 236-238.
Gere, J.M., Timoshenko, S.P., 1996. Mechanics of Materias. Chapman and Hall, London.
Goodwin, A.L., Keen, D.A., Tucker, M.G., 2008. Large negative linear compressibility of Ag-3[Co(CN)(6)]. Proc. Natl. Acad. Sci. U. S. A. 105, 18708-18713.
Grima, J.N., Attard, D., Caruana-Gauci, R., Gatt, R., 2011. Negative linear compressibility of hexagonal honeycombs and related systems. Scripta Materialia 65, 565-568.
Grima, J.N., Attard, D., Gatt, R., 2008. Truss-type systems exhibiting negative compressibility. Physica Status Solidi B-Basic Solid State Physics 245, 2405-2414.
Hall, L.J., Coluci, V.R., Galvao, D.S., Kozlov, M.E., Zhang, M., Dantas, S.O., Baughman, R.H., 2008. Sign change of Poisson's ratio for carbon nanotube sheets. Science 320, 504-507.
Lakes, R.S., Drugan, W.J., 2002. Dramatically stiffer elastic composite materials due to a negative stiffness phase? Journal of the Mechanics and Physics of Solids 50, 979-1009.
Marmier, A., Ntoahae, P.S., Ngoepe, P.E., Pettifor, D.G., Parker, S.C., 2010. Negative compressibility in platinum sulfide using density-functional theory. Physical Review B 81.
Nye, J.F., 1985. Physical properties of crystals. Clarendon press, Oxford.
Oreilly, J.C., Ritter, D.A., Carrier, D.R., 1997. Hydrostatic locomotion in a limbless tetrapod. Nature 386, 269-272.
Skelton, E.F., Feldman, J.L., Liu, C.Y., Spain, I.L., 1976. Study of Pressure-Induced Phase-Transition in Paratellurite (Teo-2). Physical Review B 13, 2605-2613.
Skvortsov, A.M., Klushin, L.I., Leermakers, F.A.M., 2007. Negative compressibility and nonequivalence of two statistical ensembles in the escape transition of a polymer chain. Journal of Chemical Physics 126.
Ting, T.C.T., Chen, T.Y., 2005. Poisson's ratio for anisotropic elastic materials can have no bounds. Quarterly Journal of Mechanics and Applied Mathematics 58, 73-82.
Weng, C.N., Wang, K.T., Chen, T., 2008. Design of microstructures and structures with negative linear compressibility in certain directions. Advances in Fracture and Materials Behavior, Pts 1 and 2 33-37, 807-813.
White, S.H., King, G.I., 1985. Molecular Packing and Area Compressibility of Lipid Bilayers. Proc.

Natl. Acad. Sci. U. S. A. 82, 6532-6536.
Yang, W., Li, Z.M., Shi, W., Xie, B.H., Yang, M.B., 2004. On auxetic materials. Journal of Materials Science 39, 3269-3279.

Figures Captions

Fig. 1: Wine-rack mechanism for structure subjected to hydrostatic pressure. Top, square structure forced by symmetry forced to compress isotropically though the members, with no hinging. Bottom, small deviation from squareness increases freedom, and hinging leads to NLC.

Fig. 2: Beam structure nomenclature: Figures a)-c) show the layout for the 2D structure where a) shows the type Ia beams, b) shows the type Ib beams and c)shows the type II beams. For the tetragonal structure d) shows the type Ia beams, e) shows the type Ib beams, f) and g) show the type IIa beams, h) shows type IIb, i) shows type III and g) and j) shows relevant angles θ and γ.

Fig. 3: Minimum absolute linear compressibility (dotted line) and minimum normalised linear compressibility (solid line) for type II beams in the 2D model across various angles of θ.

Fig. 4: Minimum absolute linear compressibility (dotted line) and minimum normalised linear compressibility (solid line) for type III beams in a tetragonal structure across different angles of θ.

Fig. 5: Minimum absolute linear compressibility (dotted line) and minimum normalised linear compressibility (solid line) for type II beams in a tetragonal structure across different angles of θ.

Fig. 6: Absolute Minimum Linear Compressibility for increasing Length: Radius ratio for the type III beam structure where the dotted line is for θ=26.6° and the dashed line is for θ=15°.

Figures

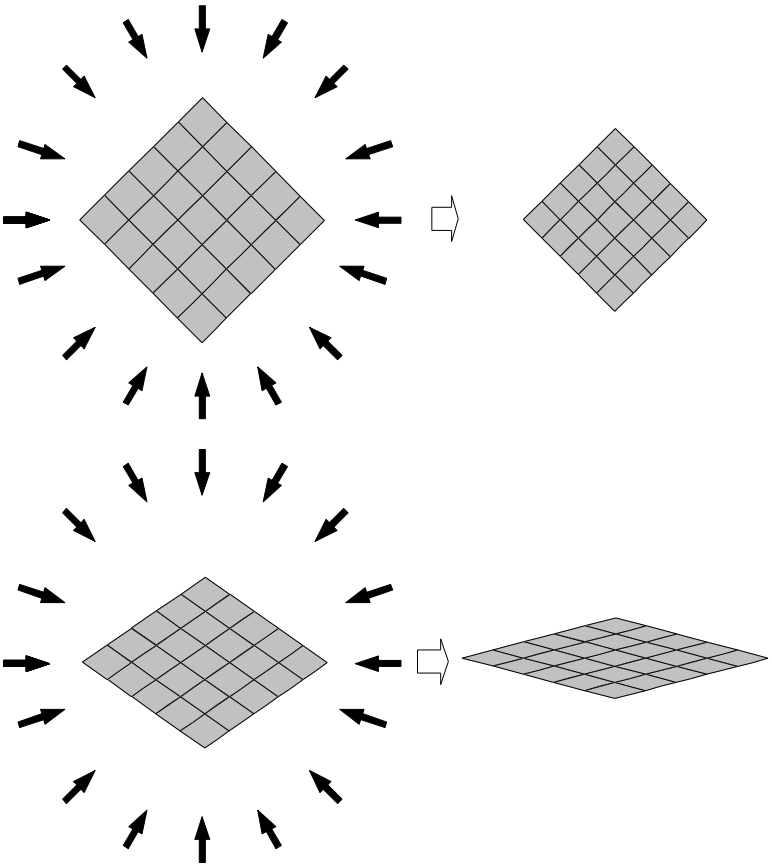

Figure 1

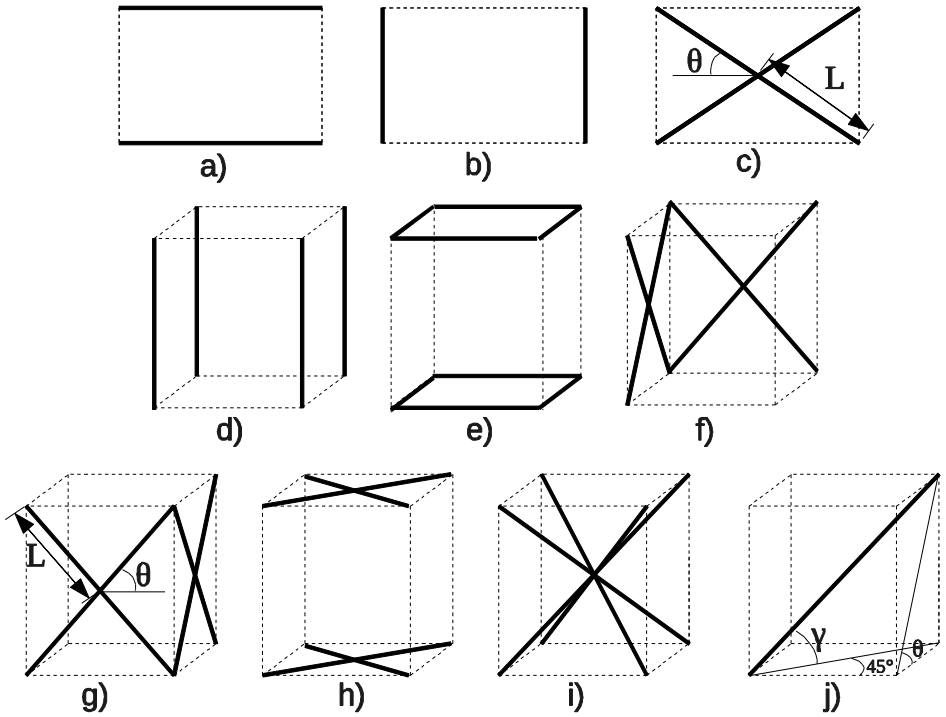

Figure 2

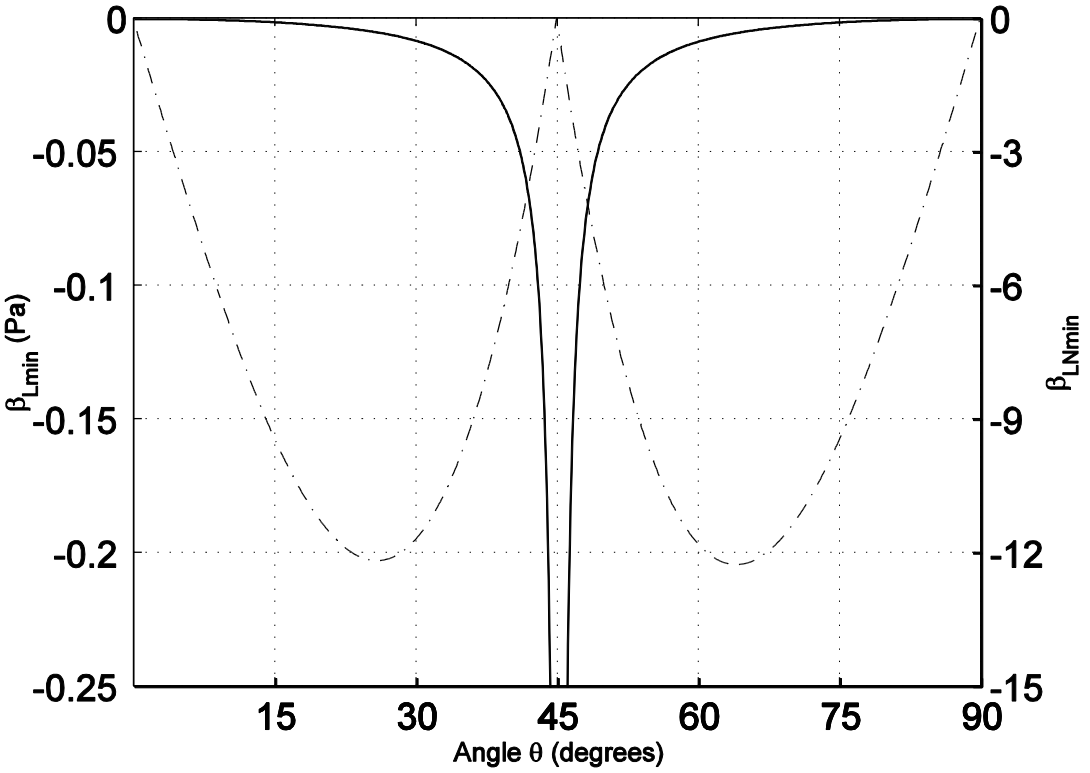

Figure 3

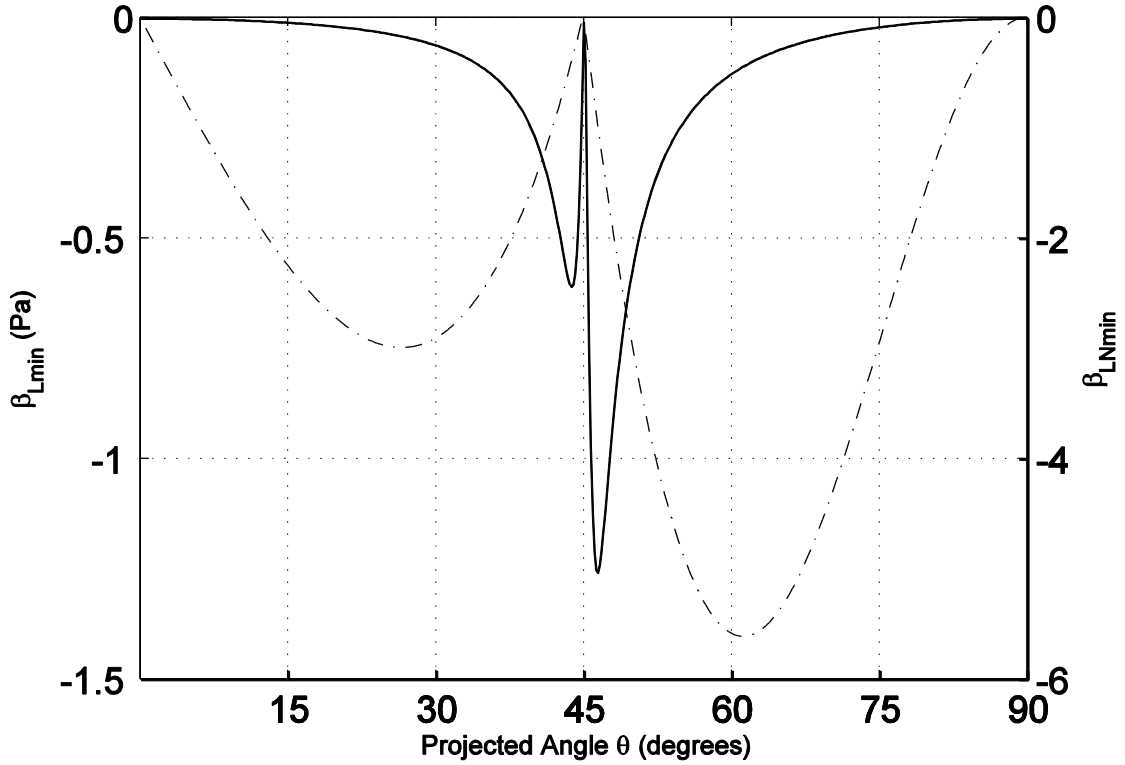

Figure 4

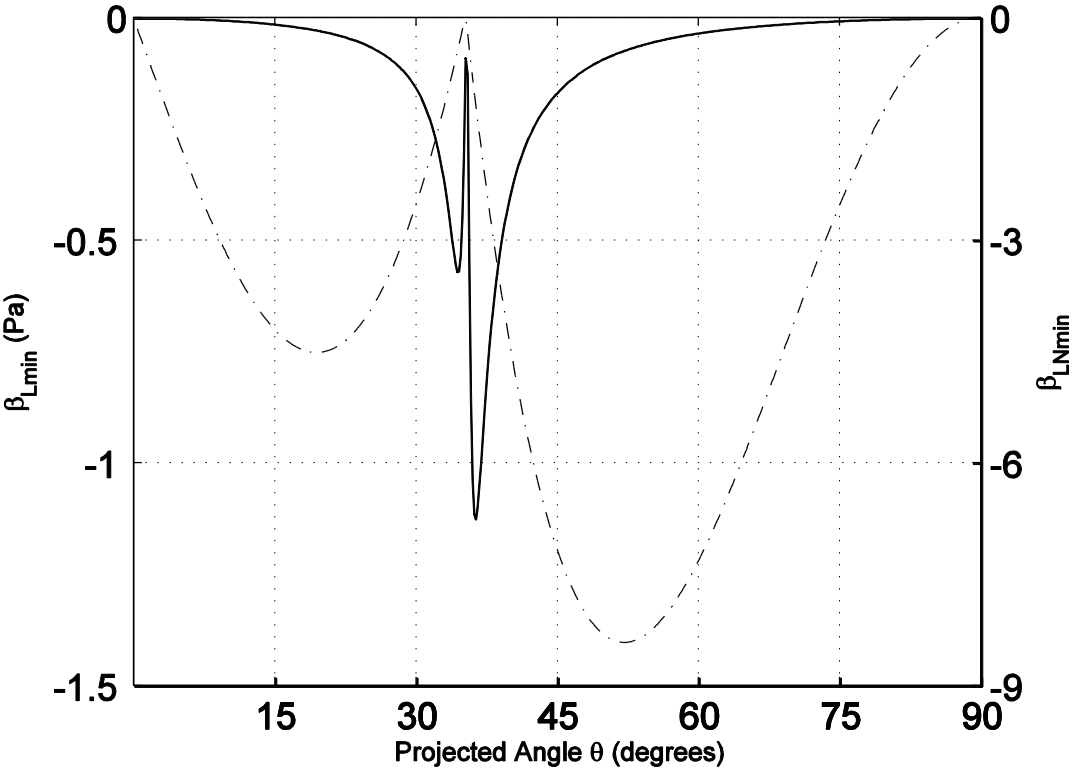

Figure 5

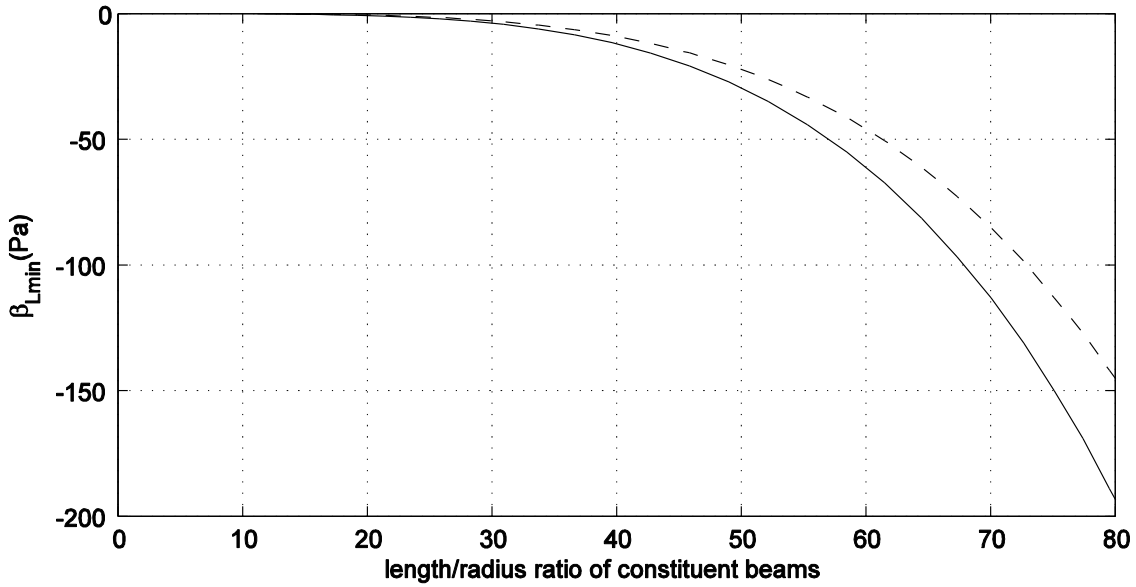
0
-50
-100
-150
-200
β_{Lmin}(Pa)
0
10
20
30
40
50
60
70
80
length/radius ratio of constituent beams

Figure 6